ACS APPLIED MATERIALS & INTERFACES

RESEARCH ARTICLE

www.acsami.org

# Tin(IV) Oxide Coatings from Hybrid Organotin/Polymer Nanoparticles

Rafael Muñoz-Espí,* Paolo Dolcet,[†,‡] Torsten Rossow,[†] Manfred Wagner, Katharina Landfester, and Daniel Crespy*

Max Planck Institute for Polymer Research, Ackermannweg 10, 55128 Mainz, Germany

Supporting Information

**ABSTRACT:** Tin dioxide coatings are widely applied in glasses and ceramics to improve not only optical, but also mechanical properties. In this work, we report a new method to prepare $SnO_2$ coatings from aqueous dispersions of polymer/organotin hybrid nanoparticles. Various liquid organotin compounds were encapsulated in polymeric nanoparticles synthesized by miniemulsion polymerization. Large amounts of tetrabutyltin and bis(tributyltin) could be successfully incorporated in cross-linked and noncross-linked polystyrene nanoparticles that served as sacrificial templates for the formation of tin oxide coatings after etching with oxygen plasma or calcination. Cross-linked polystyrene particles containing bis(tributyltin)—selected for having a high boiling point—were found to be especially suited for the oxide coating formation. The content of metal in the particles was up to 12 wt %, and estimations by thermogravimetrical indicated that at least 96% of the total organotin compound was converted to $SnO_2$. The resulting coatings were mainly identified as tetragonal $SnO_2$ (cassiterite) by X-ray diffraction, although a coexistence of this phase with orthorhombic $SnO_2$ was observed for samples prepared with bis(tributyltin).

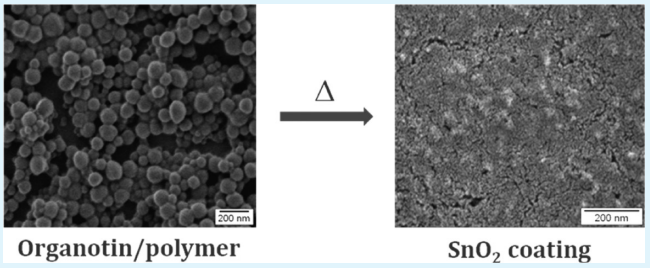


**KEYWORDS:** encapsulation, miniemulsion, nanoparticles, organotin, tin oxide

## INTRODUCTION

Tin oxide colloids have been used as pigments since ancient times. For instance, in Antic Rome they were already used in cosmetic creams, as discovered during an archeological excavation in London.[1] Tin(IV) oxide is highly transparent in the visible region of the electromagnetic spectrum, but it reflects the infrared light; combined with its low electrical resistance, these features make of $SnO_2$ a suitable material not only for advanced optoelectronic applications, such as solar cells or light emitting diodes, but also as a pigment in glasses and ceramic glazes.[2,3] In glasses and ceramics, $SnO_2$ films of different thicknesses can be applied to increase the resistance to abrasion (films of <0.1 $\mu$m),[4,5] to obtain iridescent colored layers (0.1−1.0 $\mu$m),[4] and to improve the thermal isolation (>1 $\mu$m).[4] Furthermore, $SnO_2$ is one of the most used metal oxides in gas sensors applications due to its chemical and thermal stability and its high sensibility,[6−9] and it has been also applied as catalyst support.[6,10−15]

Films of $SnO_2$ can be prepared by a variety of techniques, including wet chemical approaches,[16−19] and physical methods such as vapor deposition[20−22] or laser ablation.[23,24] It is known that when ignited, organotin compounds burn to $SnO_2$, $H_2O$, and $CO_2$.[2] Accordingly, the pyrolysis under an oxidative atmosphere of solid molecular[9,25,26] and polymeric[27,28] organotin precursors has also been applied to obtain $SnO_2$ nanoparticles. Alkynylorgantin was also used as precursor for the fabrication of self-assembled bridged hybrid materials[29] and thin films.[30] The relative amount of metal in organotin polymers can be as high as >40 wt %,[27] but the synthetic pathway of such precursors requires several demanding steps. Although liquid organotin molecular compounds can also be potentially used for the same purpose, their low flash points represent a clear limitation. This restriction could, however, be overcome by encapsulation of the liquid precursors in a polymer matrix. In this sense, the miniemulsion polymerization is probably now the most versatile method to produce functionalized polymer nanoparticles and nanocapsules.[31]

Hydrophobic[32−35] but also hydrophilic substances[36−39] can be encapsulated either in a polymer matrix ("nanoparticle"),[32−35,38,39] or dissolved or dispersed in the liquid core of a core/shell nanoparticle ("nanocapsule").[36,37] Previous work showed that silver nanoparticles can be produced in situ in miniemulsion droplets by the reduction of a silver salt. The interface of the droplets was used to perform polyaddition and polycondensation reactions,[36] or the entire volume of the droplets was subsequently polymerized by free-radical polymerization.[38] The latter method was used to encapsulate hydrophilic cobalt(II), iron(II), iron(III), nickel(II), zinc(II), and copper(II) salts in poly(2-hydroxyethyl methacrylate) particles in water-in-oil miniemulsions.[39] Owing to their rather low solubility, hydrophobic metal complexes are encapsulated in much lower amounts in oil-in-water miniemulsions (with an aqueous continuous phase) compared to their hydrophilic counterparts. This is a known problem, also typically encountered in the encapsulation of metallopharmaceutics.[40]

Received: July 22, 2011
Accepted: September 28, 2011
Published: September 28, 2011





dx.doi.org/10.1021/am200954e | ACS Appl. Mater. Interfaces 2011, 3, 4292–4298

The encapsulation of metal complexes in hydrophobic particles is particularly interesting because it makes possible the use in aqueous-based systems. Moreover, oil-in-water dispersions are usually easier to stabilize than water-in-oil ones. Hydrophobic complexes of platinum(II), indium(III), zinc(II), chromium(III), and iron(III) were encapsulated and used further for colloid lithography applications.[34,41] Almost 1 wt % of platinum(II) acetylacetonate was located in polystyrene nanoparticles fabricated in miniemulsion.[41] One strategy to increase the amount of not well-soluble substance in the disperse phase of an emulsion is to dilute the monomer and the substance to be encapsulated in a solvent that can be emulsified and later evaporated. This strategy was used to improve the dielectric constant of polyaniline/polydivinylbenzene hybrid particles.[35]

This work presents a novel approach for the formation of $SnO_2$ coatings from encapsulated liquid organotin precursors. We report for the first time—to the best of our knowledge—the encapsulation of very large amounts (up to more than 12 wt % of metal in the particles) of liquid organotin precursors in polymer nanoparticles synthesized by miniemulsion polymerization. We investigate the stability of the prepared dispersions and their suitability to form tin oxide coatings by calcination or etching with oxygen plasma.

## EXPERIMENTAL SECTION

**Materials.** Di-*n*-butyltin dilaurate (DBTDL, 95%, Sigma Aldrich), bis(2-ethyl hexanoate) tin(II) (BEHT, 95%, ABCR), tetra-*n*-butyltin (TBT, 95%, Merck), bis(tri-*n*-butyltin) (BTBT, 95%, Sigma Aldrich), bis(tri-*n*-butyltin) oxide (BTBTO, 96%, Acros Organics), $\alpha,\alpha'$-azoisobutyronitrile (AIBN, 98%, Fluka), and sodium dodecylsulfate (SDS, 99%, Roth) were used without further purification. Styrene (S, 99%, Merck) and divinylbenzene (DVB, 80%, Sigma Aldrich) were passed through an aluminum oxide column before use. The chemical structures of the different organotin compounds used in the work are displayed in Figure 1 and Figure S1 (for DBTDL and BEHT). ***Caution!*** *Tributyltin, bis(tri-n-butyltin), and bis(tri-n-butyltin) oxide are toxic chemicals and are hazardous for the health and the aquatic environment. Thus, these chemicals must be handled and disposed with care.*

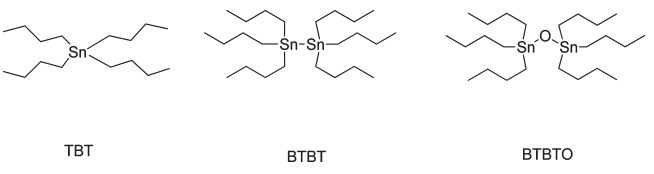


**Figure 1.** Chemical structures of the organotin precursors used in the synthesis: tetra-*n*-butyl tin (TBT), bis(tri-*n*-butyltin) (BTBT), and bis(tri-*n*-butyltin) oxide (BTBTO).

**Synthesis of Hybrid Organotin–Polymer Nanoparticles.** The monomers (styrene and divinylbenzene) were mixed with the organotin compound according to the amounts given in Table 1. After dissolving AIBN (98 ± 2 mg) in the monomer/organotin mixture, an aqueous solution of SDS (30 g of solution, 1.00 ± 0.02 $g \cdot L^{-1}$) was added. Afterward, the mixture was stirred for 1 h and ultrasonicated for 2 min with a Branson Sonifier W450 Digital (1/2 in. tip, 90% amplitude, 1 s pulse/0.1 s pause) under cooling in an ice–water bath. The resulting miniemulsion was stirred at 72 °C for 24 h in a closed round flask, cooled at room temperature, and filtered. As a representative sample for estimating the polymerization yield, the dispersion prepared with styrene and BTBT (sample **3**) was precipitated in an excess of methanol and filtered. The precipitate was dissolved in toluene, reprecipitated in methanol, and dried under vacuum. The polymerization yield was determined gravimetrically from the weight of the dry precipitate.

**Formation of $SnO_2$ Coatings.** The coatings were prepared by simple drop-casting on silicon wafers from dilutions of the miniemulsions. The silicon wafers used for the plasma etching experiments were previously treated by immersion for 2 h at 60 °C in a 3:1 mixture of concentrated ammonia with hydrogen peroxide. Plasma etching of the samples (15 sccm, 50 W power, 30 min) was performed in a plasma oven (Diener electronic Femto) and the calcination took place in a muffle furnace (Nabertherm Controller P330 LT 5/13) according to the following heating program: 25 → 500 °C with a heating rate of 3 $°C \cdot min^{-1}$, plateau of 3 h at 500 °C, and annealing to room temperature.

**Analytical Methods.** The morphology of the samples was investigated by scanning electron microscopy (Zeiss 1530 LEO Gemini, operated up to 2 kV) and transmission electron microscopy (Zeiss EM902, operated at 80 kV). The apparent molecular weight was determined by GPC using THF as an eluent and a calibration with polystyrene standards. The measurements were performed on a Waters 515 pump coupled with a refractive index detector (ERC RI 101), using 10 $\mu$m 0.8 × 30 cm SDV columns (PSS, Mainz, Germany) with 106, 104, and 500 Å with a flow rate of 1 $mL \cdot min^{-1}$ at 30 °C. Thermogravimetric analysis (TGA) was carried out with a thermobalance Mettler Toledo ThermoSTAR TGA/SDTA 851 under an air atmosphere (30 $mL \cdot min^{-1}$) with a heating rate of 10 $°C \cdot min^{-1}$ from room temperature to 900 °C. X-ray diffraction patterns were recorded on a Bruker D8 Advance 2 diffractometer with Cu K$\alpha$ radiation ($\lambda$ = 1.54 Å, 40 kV, 30 mA) in the range $2\theta$ = 5–65° ($\Delta 2\theta$ = 0.02°, $\Delta t$ = 15 s).

The $^{119}$Sn NMR spectra were performed on a Bruker Avance III 700 spectrometer at 261 MHz at 298.3 K using the topspin 3.0 software (Bruker). Quantitative tin measurement were carried out with inverse gated decoupling technique using a 30° flip angle of 6.3 $\mu$s and a recovery

**Table 1. Composition of the Organotin-Containing Dispersions, Coagulum Separated after Polymerization, and Fraction of Dispersed Phase $f_{d\varphi}$ Measured after Freeze-Drying of the Resulting Miniemulsions**

| | organotin | | monomers [g] | | | |
|---|---|---|---|---|---|---|
| sample | compound | mass [g] | styrene | DVB | coagulum[a] [g] | $f_{d\varphi}$[b] [wt %] |
| **1** | TBT | 2.00 | 4.04 | 0 | 0.27 | 15.5 |
| **2** | TBT | 2.00 | 3.84 | 0.16 | 0.44 | 12.8 |
| **3** | BTBT | 2.00 | 4.00 | 0 | 0.49 | 15.0 |
| **4** | BTBT | 2.00 | 3.85 | 0.16 | 0.32 | 16.6 |
| **5** | BTBTO | 2.10 | 4.05 | 0 | 1.99 | n.d.[c] |
| **6** | BTBTO | 2.00 | 3.84 | 0.16 | 1.89 | 9.9 |

[a] Coagulum measured after drying the feed of the filtration. [b] Fraction of dispersed phase measured by freeze-drying the filtrate and defined as the ratio of the weights of organotin + polymer + surfactant in the dispersed phase (excluding the coagulum) to the total weight of the dispersion. [c] Not determined.

Table 2. Characteristics of Organotin−Polymer Hybrid Minimemulsions

| | | | molecular weight of polymer[a] | | | | |
|---|---|---|---|---|---|---|---|
| sample | composition | $D_h$ | $M_n$ | $M_w$ | PDI[b] | organotin in the dispersed phase[c] [wt %] | organotin converted to $SnO_2$ after calcination[d] [%] |
| 1 | PS/TBT | 161 ± 75 | 55 500 | 292 000 | 5.3 | 32.6 | 45.0 |
| 2 | P(S-*co*-DVB)/TBT | 178 ± 72 | cross-linked | | | 26.0 | 5.3 |
| 3 | PS/BTBT | 142 ± 51 | 52 500 | 302 000 | 5.8 | 27.1 | 54.9 |
| 4 | P(S-*co*-DVB)/BTBT | 133 ± 52 | cross-linked | | | 32.2 | 96.0 |
| 5 | PS/BTBTO | 147 ± 25 | 221 500 | 710 500 | 3.2 | 10.4 | nd[e] |
| 6 | P(S-*co*-DVB)/BTBTO | 270 ± 160 | cross-linked | | | 6.2 | 48.0 |

[a] Determined by GPC. [b] Polydispersity index (PDI) determined by GPC. [c] Measured by $^{119}$Sn-NMR spectroscopy. [d] Estimation from the residue remaining after calcination from the TGA measurements (cf. Figure 4). [e] Not determined.

delay of 20 s. The $^{119}$Sn NMR spectra were referenced against tetrabutyltin (TBT) at −7 ppm. All the signals were obtained in the same spectral width window of 300 ppm to allow measurements under comparable conditions. A 200 mg portion of the freeze-dried samples was dissolved in 2 g of a 90:10 toluene−toluene-$d_8$ mixture in the presence of a defined amount of another organotin was taken as an internal standard (between 2 and 4 × $10^{-4}$ mol). BTBTO was used as standard for hybrid materials containing TBT, whereas TBT was the standard for samples containing BTBTO and BTBT. After optimizing the relaxation delay and the spectral width the $^{119}$Sn nuclei were integrated against the reference compound. The $^{119}$Sn chemical shifts for the tetrabutyltin, bis(tri-*n*-butyltin), and bis(tri-*n*-butyltin) oxide are −7, −80, and +85 ppm, respectively with $\delta$ = 0 ppm for tetramethyltin.

## RESULTS AND DISCUSSION

**1. Colloidal Stability of the Miniemulsions and Dispersions.** Miniemulsions with at least 30 wt % (with respect to styrene) of the different organotin compounds shown in Figure 1 were prepared in the absence and presence of divinylbenzene, used as a cross-linker. Samples prepared with DBTDL or BEHT were found to be unstable, i.e. phase separation was observed after polymerization (Supporting Information, Table S1). Differently from the other organotin compounds used in this study, DBTDL and BEHT are ionic. The destabilization may be, therefore, caused by a salting out effect resulting from the relative high ionic strength present in the system. It is known that dibutyltin dilaurate is partly hydrolyzed to lauric acid and dibutyltin dihydroxide even at room temperature, leading also to charged carboxylate species.[42]

The miniemulsions with BTBTO did also not yield stable dispersions, as can be deduced from the high amount of coagulum (cf. Table 1). This is attributed to the higher polarity and, thus, solubility of BTBTO in the continuous phase compared to TBT and BTBT. In a different manner, miniemulsions containing TBT and BTBT were found to be particularly stable.

As reported in Table 2, the hydrodynamic diameters ($D_h$) of the nanoparticles with TBT were larger than those for BTBT. TBT has a lower density (1.06 g·cm$^{-3}$ at 25 °C) than BTBT (1.15 g·cm$^{-3}$ at 25 °C) and, therefore, an equal mass of organotin in the dispersion lead to a larger droplet volume for TBT. The sizes of cross-linked nanoparticles were not significantly different from the noncross-linked analogous nanoparticles.

**2. Polymerization of the Monomers in the Presence of the Organotins.** Tetraalkyltin molecules can react with free radicals at a hydrogen center of an alkyl ligand to form stannylalkyl radicals, which can undergo a $\beta$-scission of a Sn−C bond.[43] Moreover, at temperatures as low as 100 °C, the Sn−Sn bond of some distannanes can break irreversibly and form alkyl radicals.[44] In principle, these radicals can react further with double bonds to yield new alkyl radicals or recombine to yield distannanes.[45] The chemical structure of the organotin was verified to remain intact under our experimental conditions by $^{119}$Sn NMR spectroscopy (see below), and no tin compound could be detected in the chain of polystyrene.

Taken as a representative sample, the polymerization yield of the sample prepared with styrene and BTBT (sample **3**) was estimated to be >90% from reprecipitation experiments. The molecular weight of the polymer present in stable samples, contained in Table 2, was found to be 55 500 and 52 500 g·mol$^{-1}$ for the samples with TBT (sample **1**) and BTBT (sample **3**), respectively. These values are in the typical range measured for nanocapsules produced by free-radical polymerization of styrene in miniemulsion considering the initiator concentration that was used.

**3. Encapsulation of a High Amount of Tin Oxide Precursors.** After polymerization, the organotin-containing colloids were analyzed by electron microscopy. Micrographs of the samples prepared with TBT, BTBT, and BTBTO are shown in Figure 2. No significant discrepancy was observed between the particle sizes measured by light scattering data and electron microscopy. Noncross-linked nanoparticles of TBT and BTBT displayed two kinds of morphologies: a majority of spherical nanoparticles and occasionally half-spherical larger particles (cf. insets in Figure 2). The latter morphology is explained by the different chemical composition of the droplets. In particular, droplets with higher amount of organotin can lead to acornlike droplets that transform to half spheres after the evaporation of the organotin-containing hemisphere.

The selected organotin compounds possess a high amount of tin in their chemical structures (34.2 and 40.9 wt % of Sn for TBT and BTBT, respectively). The theoretical amount of tin metal was calculated to be between 1.9 wt % (samples with TBT, **1** and **2**) and 2.3 wt % (samples with BTBT, **3** and **4**) in the aqueous dispersion. The amount of tin from TBT and BTBT precursors in the dispersed phase was determined to be between 26 and 33 wt % by $^{119}$Sn-NMR spectroscopy, that is, close to the theoretical amount of 33 wt % (Table 2, representative spectra are shown in Figure S2 of the Supporting Information). The amount was found to be much lower when BTBTO was used as precursor. Indeed, 10.4 and 6.2 wt % of BTBTO were found in the freeze-dried dispersions of PS/BTBTO and P(S-*co*-

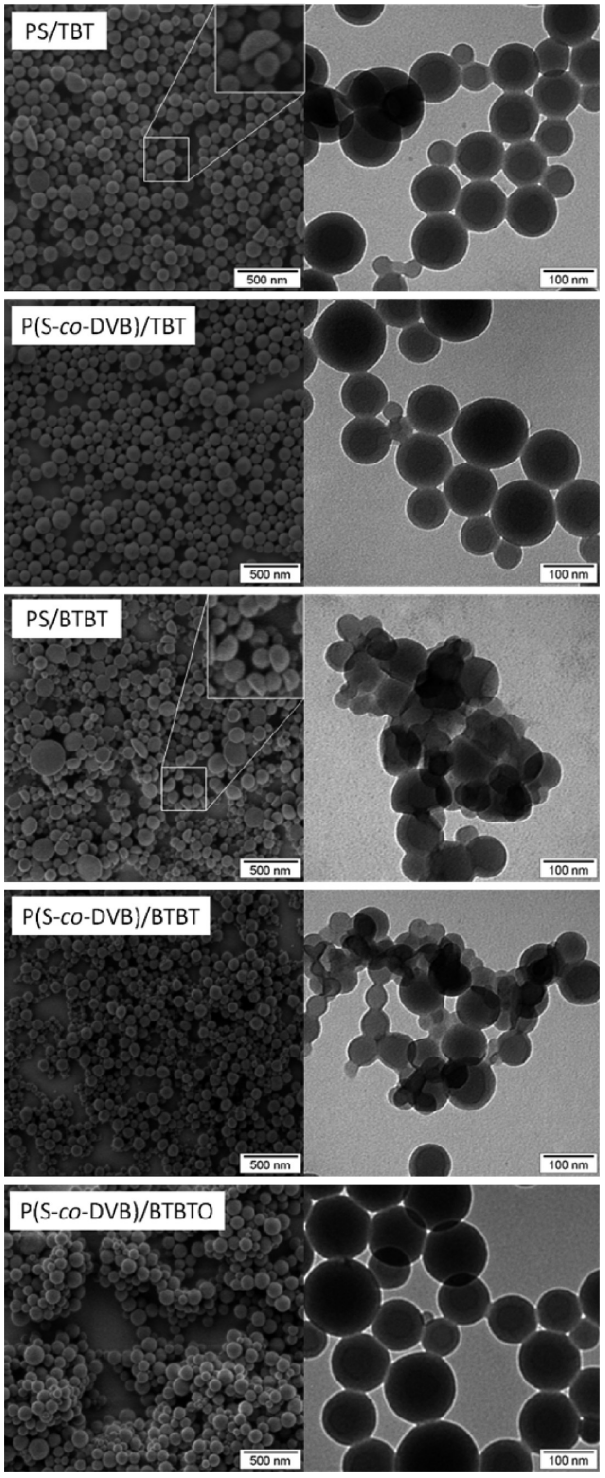


**Figure 2.** SEM (left) and TEM (right) micrographs of the organotin−polymer nanoparticles.

DVB)/BTBTO, respectively. These lower values compared to TBT- and BTBT-containing particles are explained by the large amount of coagulum and the high contents of BTBTO found in it. Quantitative $^{119}$Sn-NMR spectroscopy revealed that the BTBTO represented 42.6 wt % of the coagulum.

The amount of metal is particularly high, especially taking into account that the hybrid nanoparticles are dispersed in water. It is

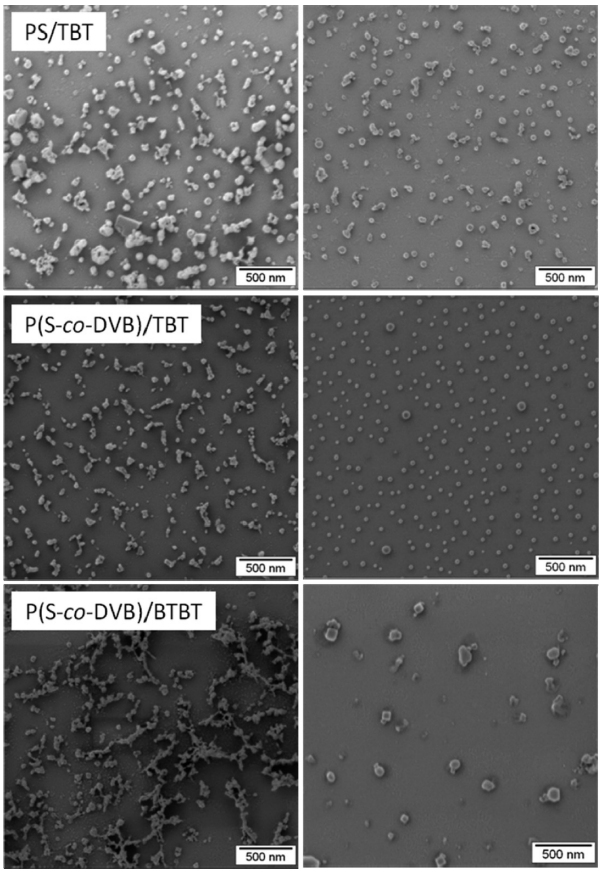


**Figure 3.** SEM micrographs of selected samples after treatment with oxygen plasma, casted from dilutions 1:200 (left) and 1:1000 (right) of the initial dispersion.

expected that a further optimization of the system could lead to dispersions with even higher content of metal.

**4. Removal of the Sacrificial Template and Formation of $SnO_2$ Coatings.** The removal of the sacrificial polymer template and the oxidation and decomposition of the organotin compounds to form $SnO_2$ coatings can be achieved by two different methods: the calcinations of the samples under an oxidative atmosphere or the etching by the use of oxygen plasma. Thermogravimetric analysis (TGA) under air of freeze-dried dispersions containing TBT, described below in more detailed, showed that the temperature of decomposition of the polymer is in the same range as the boiling point of TBT, which implies that part of the TBT will evaporate before being oxidized. Therefore, for this case, the use of oxidative plasma should be more efficient, as it has been shown in the past for platinum-containing polymer nanoparticles.[34]

Figure 3 presents SEM micrographs of samples prepared with TBT and BTBT at two different dilutions of the dispersion (1:200 and 1:1000 in water). The casting of the less diluted samples led to the formation of aggregates, although the morphology of the single nanoparticles are still recognizable (Figure 3, left). In some cases, it was possible to etch single hybrid particle by consequently diluting the dispersion before casting on the substrate (Figure 3, right). The sizes of tin oxide nanoparticles observed by microscopy were matching the theoretical diameter (20−35 nm) of $SnO_2$ nanoparticles, $D_{SnO_2}$, calculated by assuming a spherical shape and that the composition of the coagulum is

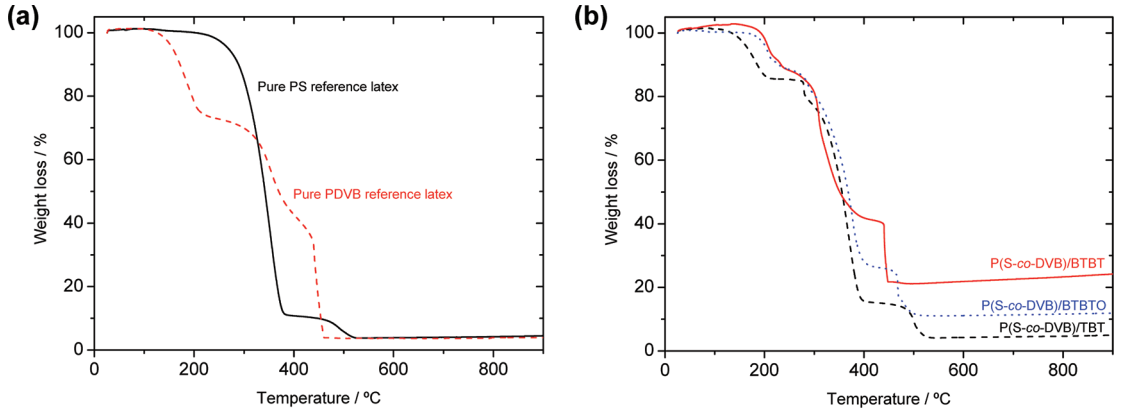


**Figure 4.** Thermogravimetric analysis (TGA) curves of freezed-dried samples: (a) reference polystyrene (PS) and polydivinylbenzene (PDVB) latexes; (b) cross-linked samples prepared with TBT, BTBT, and BTBTO.

the same as the composition of the dispersed phase according to

$$D_{SnO_2} = D_{droplet} \sqrt[3]{\frac{M_{SnO_2}}{\rho_{SnO2} M_{OT}} \frac{m_{OT}}{\frac{m_{OT}}{\rho_{OT}} + \frac{m_p}{\rho_p}}}$$

where $D_{droplet}$ is the diameter of the droplet; $\rho_{OT}$, $\rho_p$, and $\rho_{SnO_2}$ are the densities of the organotin compound (1.06 and 1.15 $g \cdot cm^{-3}$ at 25 °C for TBT and BTBT), the polymer (1.04 $g \cdot cm^{-3}$ at 25 °C for polystyrene), and cassiterite (7.15 $g \cdot cm^{-3}$ at 25 °C); $M_i$ is the molar mass of the species; and $m_i$ is the mass of the species in the sample. The average sizes of the nanoparticles were found to range between 24 nm for sample 6 and 44 nm for sample 2 (Figure S3, Supporting Information).

The inorganic nanoparticles from noncross-linked particles (cf. Figure 3, PS/TBT) present some aggregates even in the low concentration regime, which is caused by an easier coalescence during heating in comparison to the more rigid cross-linked particles, (cf. Figure 3, P(S-*co*-DVB)/TBT and P(S-*co*-DVB)/BTBT).

Although plasma etching is excellently suited for lower concentrations, the method was not as efficient when higher concentrations (i.e., thicker films of the inorganic oxide) are required, because the polymer could not be completely removed. The calcination is clearly a more convenient strategy for obtaining thicker films, although it may have efficiency limitations with organotin compounds with a boiling point close to the thermal decomposition of the polymer, as mentioned above.

Prior to pyrolysis of the samples, the thermal decomposition of the hybrid samples was studied by TGA under an air atmosphere. After calcination, the remaining residue should be essentially composed of $SnO_2$ (and minor rests of carbon due to the polymer degradation). Subsequently, from the percentages of the remaining residue, we can estimate the fraction of the initially introduced organotin that converts to $SnO_2$ after calcination. The last column of Table 2 contains the results of this estimation. By observing the values, there are two especially remarkable aspects: first, the higher efficiency of the conversion of the noncross-linked TBT-containing sample to $SnO_2$ (45.0%), when compared with the cross-linked one (only 5.3%); and second, the almost complete conversion (96.0%) for the P(S-*co*-DVB)/BTBT sample. The latter is not surprising if we take into account the high boiling point of BTBT and the efficient encapsulation of the organotin in cross-linked capsules. For understanding the first observation, it is helpful to have a look to the thermal decomposition of reference PS and PDVB latexes, depicted in Figure 4a. The PS latex starts decomposing at about 250 °C, whereas the PDVB latex does it at about 140 °C. PDVB may decompose simultaneously to the evaporation of TBT, degrading the cross-linked P(S-*co*-DVB) shell and facilitating the evaporation of the encapsulated precursor, which results in a very low conversion to $SnO_2$. On the contrary, the efficiency will be higher with pure PS particles, even if they are not cross-linked, because they start to degrade at a higher temperature. This explanation is confirmed by the fact that 26.0 wt % of TBT could be found in the dispersed phase by $^{119}Sn$ NMR spectroscopy before the calcination (Table 2). To illustrate the differences between the different organotin precursors, Figure 4b contains the TGA traces of the cross-linked samples prepared with TBT, BTBT, and BTBTO.

The success of the calcination strategy could be demonstrated by calcinating at 500 °C (temperature at which the polymer has been completely removed and only $SnO_2$ remains, according to TGA data) samples prepared with high and low concentrations of the hybrid dispersions. EDX spectra indicated that the coatings are slightly contaminated with carbon originating from the calcination of the polymer (Figure S4, Supporting Information). Figure 5 shows the micrographs of tin oxide coatings formed after calcinations of samples with the different precursors. The casting of the as-prepared dispersions lead to thicker oxide films (Figure 5, left) and high dilutions resulted in the formation of inorganic nanoparticles from single hybrid precursor particles (Figure 5, right). The thickness of the prepared coatings was estimated with a profilometer and could be varied between ca. 100 nm and up to 500 nm, depending on the concentration of the casted dispersion. The sizes of nanoparticles produced by plasma etching and by calcination are similar.

X-ray diffraction patterns of the calcinated samples, shown in Figure 6, confirmed that the formed coatings were crystalline. The reflections can be clearly identified with those of tetragonal $SnO_2$ (cassiterite, JCPDS card. No. 41−1445). However, in the coatings prepared with dispersions containing BTBT, the thermodynamically stable tetragonal phase coexists with an orthorhombic $SnO_2$ phase, normally formed under high-pressure conditions. The appearance of the orthorhombic phase in $SnO_2$ films prepared under oxygen deficiency conditions has been previously reported,[46,47] and may be related with the formation of a litharge phase of SnO that transform to the orthorhombic form and not

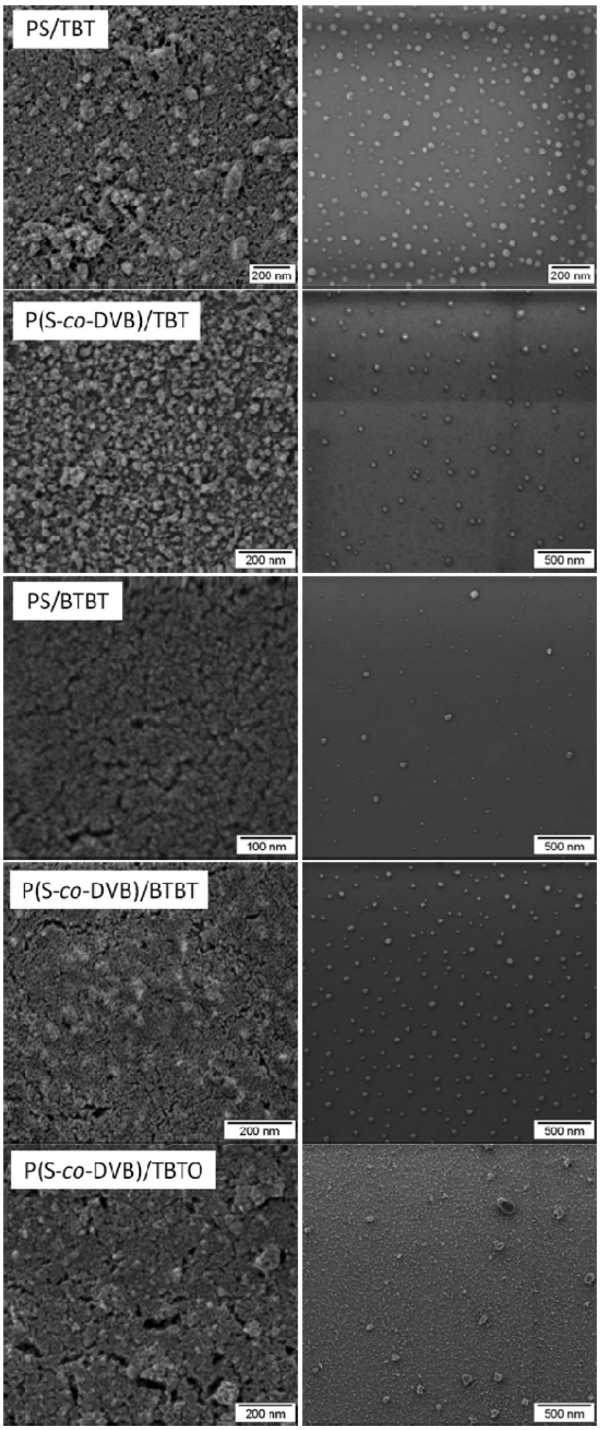


**Figure 5.** SEM micrographs of the samples after calcinations at 500 °C. Dispersions were casted as prepared (left) and at a dilution 1:30 (right).

to the stable cassiterite phase. The coexistence of the tetragonal and the orthorhombic phases only occurred in the BTBT samples, which can be explained as follows. As each molecule of BTBT contains two atoms of tin, the oxygen required for oxidation to $SnO_2$ is double than for TBT, so that an SnO intermediate phase could be formed if the oxygen is not sufficient during the calcination process. In BTBTO, the two Sn atoms are linked with an oxygen and the oxygen required for oxidation is equivalent to TBT. The size of the crystalline domains was

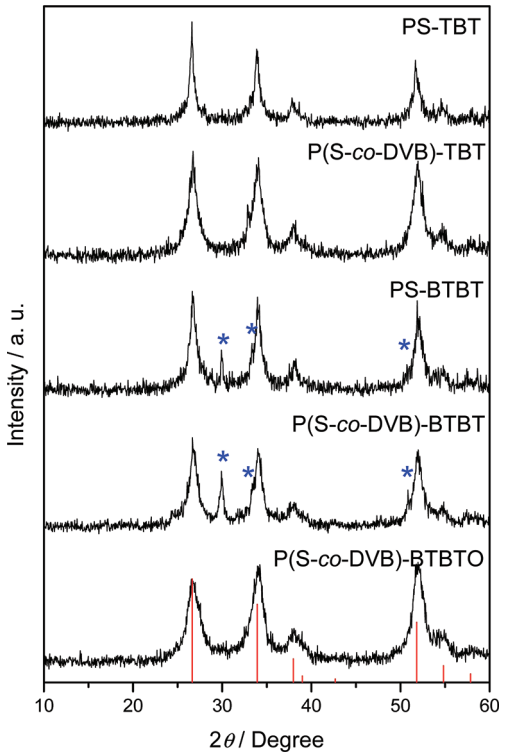


**Figure 6.** X-ray diffraction patterns of the samples prepared by casting the dispersions on silicon wafers and subsequent calcination at 500 °C. Te drop lines indicate the position and relative intensity of cassiterite (JCPDS card No. 41-1445). The peaks marked with an asterisk (*) are attributed to the presence of orthorhombic $SnO_2$ (JCPDS card No. 85-0423).

estimated to range from 5 to 17 nm by using the Scherrer equation for the (110) reflections of cassiterite in the XRD patterns.

## CONCLUSIONS

Miniemulsion polymerization has been shown to be a suitable technique for encapsulating liquid organotin precursors that can be converted to tin(IV) oxide either by etching with oxygen plasma or by calcinations under an oxidative atmosphere. From the different liquid organotin compounds screened, tetra-*n*-butyltin (TBT) and bis(tributyltin) (BTBT) form the most stable dispersions. TBT and BTBT can be successfully encapsulated in amounts as high as more than 30 wt % in polystyrene or poly(styrene-*co*-divinylbenzene) nanoparticles. This new approach is particularly interesting because the tin precursors are dispersed and processed in water. The resulting aqueous organotin/polymer dispersions can be easily coated and the thickness of the oxide coating obtained after etching can be simply adjusted by dilution of the initial dispersion. Estimations by thermogravimetric analysis demonstrated the efficiency of the method: for particles prepared with BTBT and poly(styrene-*co*-divinylbenzene) almost the whole initially introduced organotin (96%) could be transformed to $SnO_2$. X-ray diffraction confirmed the crystallinity of the prepared coating. The prepared coating were confirmed to be crystalline by X-ray diffraction and mainly identified as tetragonal $SnO_2$ (cassiterite), although a coexistence of this phase with orthorhombic $SnO_2$ was found in samples prepared with BTBT. The method can be, in principle, applied to

other hydrophobic organometallic liquids for the preparation of metal oxides coatings.

## ■ ASSOCIATED CONTENT

**Supporting Information.** Description of miniemulsions with di-*n*-butyltin dilaurate and bis(2-ethyl hexanoate) tin(II) as tin oxide precursors, $^{119}$Sn NMR spectroscopy of the organotin−polymer nanoparticles, determination of the particle size distribution of tin oxide nanoparticles from SEM measurements, and EDX measurements on calcinated organotin−polymer hybrid nanoparticles. This material is available free of charge via the Internet at http://pubs.acs.org.

## ■ AUTHOR INFORMATION

### Corresponding Author

*E-mail: munoz@mpip-mainz.mpg.de, crespy@mpip-mainz.mpg.de.

### Present Addresses

‡Also at Dipartimento di Scienze Chimiche, Università di Padova, Via Marzolo 1, 35131 Padua, Italy.

### Author Contributions

†These two authors contributed equally to this work.

## ■ ACKNOWLEDGMENT

We thank Gunnar Glaser and Dr. Ingo Lieberwirth for their suggestions and assistance with the electron microscopy and EDX analysis, Sandra Seywald for the GPC measurements, and Michael Bach for the XRD measurements. P.D. thanks the Ph.D. School in Molecular Sciences of the University of Padua for financial support.

## ■ REFERENCES

(1) Evershed, R. P.; Berstan, R.; Grew, F.; Copley, M. S.; Charmant, A. J. H.; Barham, E.; Mottram, H. R.; Brown, G. *Nature* **2004**, *432*, 35–36.
(2) Greenwood, N. N.; Earnshaw, A. *Chemistry of the Elements*, 2nd ed.; Butterworth-Heinemann: Oxford, 1997.
(3) Batzill, M.; Diebold, U. *Prog. Surf. Sci.* **2005**, *79*, 47–154.
(4) Holleman, A. F.; Wiberg, E. *Lehrbuch der Anorganischen Chemie*, 102 ed.; De Gruyter: Berlin, 2007.
(5) Budd, S. M. *Thin Solid Films* **1981**, *77*, 13–20.
(6) Diebold, U.; Batzill, M. *Prog. Surf. Sci.* **2005**, *79*, 47–154.
(7) Ihokura, K.; Watson, J. *The Stannic Oxide Gas Sensor: Principles and Applications*; CRC Press: FL, 1994.
(8) Barsan, N.; Schweizer-Berberich, M.; Gopel, W. *Fresenius J. Anal. Chem.* **1999**, *365*, 287–304.
(9) Nayral, C.; Viala, E.; Fau, P.; Senocq, F.; Jumas, J. C.; Maisonnat, A.; Chaudret, B. *Chem.—Eur. J.* **2000**, *6*, 4082–4090.
(10) Gopel, W.; Schierbaum, K. D. *Sensors Actuat. B−Chem.* **1995**, *26*, 1–12.
(11) Law, M.; Kind, H.; Messer, B.; Kim, F.; Yang, P. D. *Angew. Chem., Int. Ed.* **2002**, *41*, 2405–2408.
(12) Kolmakov, A.; Zhang, X. Y.; Cheng, G. S.; Moskovits, M. *Adv. Mater.* **2003**, *15*, 997.
(13) Lee, K. S.; Park, I. S.; Cho, Y. H.; Jung, D. S.; Jung, N.; Park, H. Y.; Sung, Y. E. *J. Catal.* **2008**, *258*, 143–152.
(14) Sekizawa, K.; Widjaja, H.; Maeda, S.; Ozawa, Y.; Eguchi, K. *Appl. Catal., A* **2000**, *200*, 211–217.
(15) Yamaguchi, N.; Kamiuchi, N.; Muroyama, H.; Matsui, T.; Eguchi, K. *Catal. Today* **2011**, *164*, 169–175.
(16) Niederberger, M.; Pinna, N. *Metal Oxide Nanoparticles in Organic Solvents*; Springer: Dordrecht, 2009.
(17) Juttukonda, V.; Paddock, R. L.; Raymond, J. E.; Denomme, D.; Richardson, A. E.; Slusher, L. E.; Fahlman, B. D. *J. Am. Chem. Soc.* **2006**, *128*, 420–421.
(18) Deng, Z. T.; Peng, B.; Chen, D.; Tang, F. Q.; Muscat, A. J. *Langmuir* **2008**, *24*, 11089–11095.
(19) Ba, J. H.; Polleux, J.; Antonietti, M.; Niederberger, M. *Adv. Mater.* **2005**, *17*, 2509–+.
(20) Liu, Y.; Koep, E.; Liu, M. L. *Chem. Mater.* **2005**, *17*, 3997–4000.
(21) Rosental, A.; Tarre, A.; Gerst, A.; Uustare, T.; Sammelselg, V. *Sens. Actuator B−Chem.* **2001**, *77*, 297–300.
(22) Sun, S. H.; Meng, G. W.; Zhang, G. X.; Masse, J. P.; Zhang, L. *Chem.—Eur. J.* **2007**, *13*, 9087–9092.
(23) Hu, J. Q.; Bando, Y.; Liu, Q. L.; Golberg, D. *Adv. Funct. Mater.* **2003**, *13*, 493–496.
(24) Ristoscu, C.; Cultrera, L.; Dima, A.; Perrone, A.; Cutting, R.; Du, H. L.; Busiakiewicz, A.; Klusek, Z.; Datta, P. K.; Rose, S. R. *Appl. Surf. Sci.* **2005**, *247*, 95–100.
(25) Toupance, T.; Elhamzaoui, H.; Jousseaume, B.; Riague, H.; Saadeddin, I.; Campet, G.; Brotz, J. *Chem. Mater.* **2006**, *18*, 6364–6372.
(26) Molloy, K. C. *J. Chem. Res.* **2008**, *10*, 549–554.
(27) Tamai, T.; Ichinose, N. *Macromolecules* **2000**, *33*, 2505–2508.
(28) Tamai, T.; Ichinose, N.; Agari, Y. *Macromol. Rapid Commun.* **1999**, *20*, 179–181.
(29) Elhamzaoui, H.; Jousseaume, B.; Riague, H.; Toupance, T.; Dieudonne, P.; Zakri, C.; Maugey, M.; Allouchi, H. *J. Am. Chem. Soc.* **2004**, *126*, 8130–8131.
(30) Renard, L.; Elhamzaoui, H.; Jousseaume, B.; Toupance, T.; Laurent, G.; Ribot, F.; Saadoui, H.; Brotz, J.; Fuess, H.; Riedel, R.; Gurlo, A. *Chem. Commun.* **2011**, *47*, 1464–1466.
(31) Crespy, D.; Landfester, K. *Beilstein J. Org. Chem.* **2010**, *6*, 1132–1148.
(32) Erdem, B.; Sudol, E. D.; Dimonie, V. L.; El-Aasser, M. S. *J. Polym. Sci., Polym. Chem.* **2000**, *38*, 4431–4440.
(33) Joumaa, N.; Lansalot, M.; Theretz, A.; Elaissari, A. *Langmuir* **2006**, *22*, 1810–1816.
(34) Manzke, A.; Pfahler, C.; Dubbers, O.; Plettl, A.; Ziemann, P.; Crespy, D.; Schreiber, E.; Ziener, U.; Landfester, K. *Adv. Mater.* **2007**, *19*, 1337–1341.
(35) Molberg, M.; Crespy, D.; Rupper, P.; Nuesch, F.; Manson, J. A. E.; Lowe, C.; Opris, D. M. *Adv. Funct. Mater.* **2010**, *20*, 3280–3291.
(36) Crespy, D.; Stark, M.; Hoffmann-Richter, C.; Ziener, U.; Landfester, K. *Macromolecules* **2007**, *40*, 3122–3135.
(37) Crespy, D.; Landfester, K. *Macromol. Chem. Phys.* **2007**, *208*, 457–466.
(38) Crespy, D.; Landfester, K. *Polymer* **2009**, *50*, 1616–1620.
(39) Cao, Z. H.; Wang, Z.; Herrmann, C.; Ziener, U.; Landfester, K. *Langmuir* **2010**, *26*, 7054–7061.
(40) Crespy, D.; Landfester, K.; Schubert, U. S.; Schiller, A. *Chem. Commun.* **2010**, *46*, 6651–6662.
(41) Schreiber, E.; Ziener, U.; Manzke, A.; Plettl, A.; Ziemann, P.; Landfester, K. *Chem. Mater.* **2009**, *21*, 1750–1760.
(42) Yokoyama, T.; Kinjo, N.; Mukai, J. *J. Appl. Polym. Sci.* **1984**, *29*, 1951–1958.
(43) Davies, A. G. *Organotin Chemistry*; VCH: Weinheim, 1997.
(44) Buschhaus, H. U.; Neumann, W. P. *Angew. Chem.-Int. Ed. Engl.* **1978**, *17*, 59–59.
(45) Omae, I. *Organotin Chemistry*; Elsevier Science Publishers: Amsterdam, 1989.
(46) Shek, C. H.; Lai, J. K. L.; Lin, G. M.; Zheng, Y. F.; Liu, W. H. *J. Phys. Chem. Solids* **1997**, *58*, 13–17.
(47) Lamelas, F. J.; Reid, S. A. *Phys. Rev. B* **1999**, *60*, 9347–9351.